Dalton Transactions

PAPER

View Article Online
View Journal | View Issue

Cite this: *Dalton Trans.*, 2019, **48**, 4696

[Pb{Mn(CO)$_5$}$_3$][AlCl$_4$]: a lead-manganese carbonyl with AlCl$_4$-linked PbMn$_3$ clusters†

Silke Wolf, [a] Dieter Fenske,[a] Wim Klopper [b] and Claus Feldmann *[a]

Received 22nd January 2019,
Accepted 9th March 2019

DOI: 10.1039/c9dt00309f

rsc.li/dalton

[Pb{Mn(CO)$_5$}$_3$][AlCl$_4$] containing a trigonal planar PbMn$_3$ cluster was obtained by the reaction of PbCl$_2$ and Mn$_2$(CO)$_{10}$ in the ionic liquid [BMIm][AlCl$_4$]. The title compound is composed of [Pb{Mn(CO)$_5$}$_3$]$^+$ carbonyl cations and [AlCl$_4$]$^-$ anions that are connected to infinite zig-zag chains. The [Pb{Mn(CO)$_5$}$_3$]$^+$ cation exhibits a central PbMn$_3$ cluster with three equal Pb–Mn single bonds, resulting in an almost equilateral triangle of three manganese atoms with a formal Pb^{+I} in its center. Such a cluster and compound were identified for the first time. In addition to single-crystal structure analysis, the composition, structure and properties were further characterized by density functional theory (DFT) calculations, energy dispersive X-ray spectroscopy (EDXS), and Fourier-transform infrared spectroscopy (FT-IR), as well as optical spectroscopy (UV-Vis).

Introduction

Due to their high redox stability, ionic liquids meanwhile have turned out to be versatile reaction media for the synthesis of metal clusters and reactive carbonyl compounds.[1] Prominent examples include, for instance, □$_{24}$Ge$_{136}$ as a new modification of germanium (□ indicating non-occupied lattice sites),[2] [Hg$_4$Te$_8$(Te$_2$)$_4$]$^{8-}$ with a porphyrin-analogous structure,[3] or the Zintl-like cation [CuBi$_8$]$^{3+}$.[4] In addition to the excellent redox stability of ionic liquids, their weakly coordinating properties and the inherent stabilization of compounds *via* cation–anion interactions are further merits.[5]

With our studies on the reactivity of metal carbonyls, we could show that ionic liquids also represent powerful liquid media to obtain novel carbonyl compounds and clusters.[1b] Selected examples comprise, for instance, the adamantane-type Fe$_4$Sn$_6$ cluster in [{Fe(CO)$_3$}$_4${SnI}$_6$I$_4$]$^{2-}$,[6a] the Ge$_{12}$Fe$_8$ germanium-iron cluster in Ge$_{12}${Fe(CO)$_3$}$_8$(μ-I)$_4$ [6b] or the anti-(WCl$_2$)$_6$-like [(Pb$_6$I$_8$){Mn(CO)$_5$}$_6$]$^{2-}$.[6c] In particular, by the reaction of Fe(CO)$_5$ with Lewis-acidic metal iodides (*e.g.*, SnI$_4$, GeI$_4$), we could identify several novel carbonyl compounds that are specifically designated by the absence of alkyl and aryl ligands.[6a,b,7] Such organic ligands were often considered essential for electronic and steric stabilization of carbonyl compounds.[8] In this regard, the specific features of the ionic liquids allow preparation and stabilization of highly reactive carbonyl compounds and metal clusters that contain additional, even more destabilizing halogenide ligands.[8]

Based on our experience with the Fe–Sn and Fe–Ge system, we have expanded our studies to the Pb–Mn system. In principle, Pb–Mn bonding is well-known for carbonyl clusters and was intensely studied in regard to the structural, magnetic, catalytic and optical properties of the resulting compounds.[9] Most often isolated Pb–Mn or Mn–Pb–Mn strings were described. Larger Pb–Mn arrangements are rare and limited to Pb{=Mn(CO)$_2$Cp}{-Mn$_2$(CO)$_4$Cp$_2$} (Cp: η^5-C$_5$H$_4$CH$_3$).[10] This compound is featured by a planar PbMn$_3$ unit that exhibits two Pb–Mn single bonds as well as a significantly shorter Pb=Mn double bond. In addition, a covalent Mn–Mn bond was assumed by the authors between the two Mn atoms with Pb–Mn single bonds. As discussed above,[8] halogenide-coordinated Pb–Mn clusters were considered as highly reactive and require alkyl-/aryl-ligands for electronic and steric stabilization, since halogenide ligands were described to cause a cleavage of the Pb–Mn bonds.[11] This background motivated us to evaluate the feasibility of ionic liquids for obtaining novel carbonyl clusters with Pb–Mn bonding. This results in the synthesis of [Pb{Mn(CO)$_5$}$_3$][AlCl$_4$] containing a [Pb{Mn(CO)$_5$}$_3$]$^+$ carbonyl cation with a trigonal planar PbMn$_3$ cluster and three equal Pb–Mn single bonds.

Results and discussion

[Pb{Mn(CO)$_5$}$_3$][AlCl$_4$] was obtained by reacting PbCl$_2$ and Mn$_2$(CO)$_{10}$ in a mixture of [BMIm]Cl and AlCl$_3$ (1 : 1). Although, in principle, large quantities were obtained, the title

[a]*Institute of Inorganic Chemistry, Karlsruhe Institute of Technology (KIT), Engesserstraße 15, 76131 Karlsruhe, Germany. E-mail: claus.feldmann@kit.edu*
[b]*Institute of Physical Chemistry, Karlsruhe Institute of Technologie (KIT), Fritz-Haber-Weg 2, D-76131 Karlsruhe, Germany*

†CCDC 1890307. For crystallographic data in CIF or other electronic format see DOI: 10.1039/c9dt00309f

compound formed only very small dark red, almost black crystals that were found on the surface of large blue, rod-shaped crystals of $[Mn(CO)_6][AlCl_4]$ as a side phase. $[Mn(CO)_6][AlCl_4]$ was described already,[12] and its composition was confirmed here as well by single-crystal structure analysis. Taken together, the formation of the title compound can be rationalized by a redox reaction with reduction of Pb^{+II} to Pb^{+I} and oxidation of Mn^0 to $Mn^{+I/+II}$ according to the following equation:

$$11\,Mn_2^{\pm 0}(CO)_{10} + 6\,Pb^{+II}Cl_2 + 8[AlCl_4]^- \rightarrow 6\left[Pb^{+I}\left\{Mn^{\pm 0}(CO)_5\right\}_3\right][AlCl_4] + 2\left[Mn^{+I}(CO)_6\right][AlCl_4] + 2\,Mn^{+II}(CO)_4Cl_2 + 8\,Cl^-.$$

From the obtained products, $Mn(CO)_4Cl_2$ completely remained in solution, whereas $[Mn(CO)_6][AlCl_4]$ shows partial crystallization. Due to its solubility and being driven by Ostwald ripening, only a few bluish crystals appear that grow to millimeter-sized individuals. The title compound $[Pb\{Mn(CO)_5\}_3][AlCl_4]$ is most insoluble in the system, and thus, formed small crystals on the surface of the large seed crystals of the co-product. Since the reactivity of $[Pb\{Mn(CO)_5\}_3][AlCl_4]$ (title compound) and $[Mn(CO)_6][AlCl_4]$ (co-product) is very similar, separation is difficult and was here performed by manual separation of crystals. According to single-crystal structure determination, $[Pb\{Mn(CO)_5\}_3][AlCl_4]$ crystallizes monoclinically with the space group $P2_1/c$ (Table 1, Fig. 1).

The title compound consists of $[Pb\{Mn(CO)_5\}_3]^+$ cations and $[AlCl_4]^-$ anions. The $[Pb\{Mn(CO)_5\}_3]^+$ cation is composed of a central Pb atom, which is connected to three $Mn(CO)_5$ fragments (Fig. 2). Herein, Pb–Mn distances of 275.0(1) (Pb–Mn3) to 278.5(1) pm (Pb–Mn2) are observed (Table 2). Based on this equidistant connectivity and Mn–Pb–Mn angles of 117.7(1) (Mn2–Pb–Mn3) to 121.9(1)° (Mn1–Pb–Mn3), an almost ideal trigonal planar $PbMn_3$ arrangement is formed (Fig. 2). The Pb–Mn distances clearly point to three covalent single bonds and fit well with Pb^{+I}–Mn single bonds (279.9–281.2 pm) in $[Pb_6I_8\{Mn(CO)_5\}_6]^{2-}$.[6c] Electron counting with three Pb–Mn electron-pair bonds results in three Pb-allocated electrons, and thus, a formal oxidation state of Pb^{+I} for the group 14 element Pb. Naturally, the Pb–Mn distances in the title compound are significantly longer than the Pb^0=Mn double bond (249.0 pm) in $Pb\{Mn(CO)_2Cp\}_3$ (Fig. 3).[10] Certain

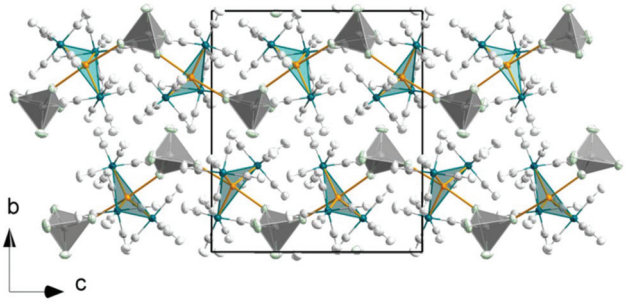

Fig. 1 Unit cell of $[Pb\{Mn(CO)_5\}_3][AlCl_4]$: $PbMn_3$ units in yellow-green, $[AlCl_4]^-$ tetrahedra in grey, and C atoms and O atoms of CO ligands in light grey.

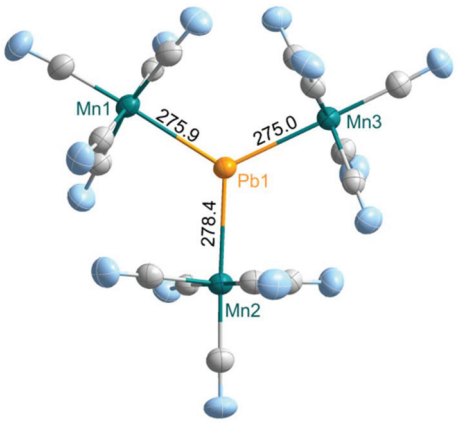

Fig. 2 Structure of the $[Pb\{Mn(CO)_5\}_3]^+$ cation (Pb–Mn distances in pm; ellipsoids comprise 50% of the probability density of the atoms).

Table 1 Crystallographic data and refinement details of $[Pb\{Mn(CO)_5\}_3][AlCl_4]$

Data	$[Pb\{Mn(CO)_5\}_3][AlCl_4]$
Sum formula	$C_{15}O_{15}AlCl_4Mn_3Pb$
Molar mass	960.95 g mol^{-1}
Crystal system	Monoclinic
Space group	$P2_1/c$ (no. 14)
Lattice parameters	a = 1020.8(2) pm
	b = 1762.0(3)pm
	c = 1791.5(5)pm
	β = 120.9(1)°
Cell volume	$V = 2763.8 \times 10^6$ pm^3
Formula units per cell	Z = 4
Calculated density	ρ = 2.309 g cm^{-3}
Measurement limits	$-13 \le h \le 12$, $-18 \le k \le 23$, $-9 \le l \le 23$
Theta range for data collection	3.32 to 64.34°
Measurement conditions	Stoe Stadivari diffractometer (Stoe)
	λ(Ga-Kα) = 134 pm, T = 150 K
Linear absorption coefficient	μ = 17.89 mm^{-1}
Number of reflections	17 417 (independent 14 261)
Refinement method	Full-matrix least-squares on F^2
Merging	R_{int} = 0.0233
Number of parameters	352
Residual electron density	3.23 to −0.82 e$^-$ 10^{-6} pm^{-3}
Figures of merit	R_1 ($I \ge 4\sigma_I$) = 0.0325
	R_1 (all data) = 0.0344
	wR_2 (all data) = 0.0889
	GooF = 0.998

Table 2 Selected distances of $[Pb\{Mn(CO)_5\}_3][AlCl_4]$ in comparison with literature data

Compound	Pb–Mn (pm)	Pb–Cl (pm)
$[Pb\{Mn(CO)_5\}_3][AlCl_4]$ (this work)	275.0(1)–278.5(1)	313.9(2), 334.4(2)
$Pb\{Mn(CO)_2Cp\}_3$ [10]	261.1–262.0 (single bond)	—
	249.0 (double bond)	—
$[(Pb_6I_8)\{Mn(CO)_5\}_6]^{2-}$ [6c]	279.9–281.2	—
$PbCl_2$ [18]	—	284.7, 308.4

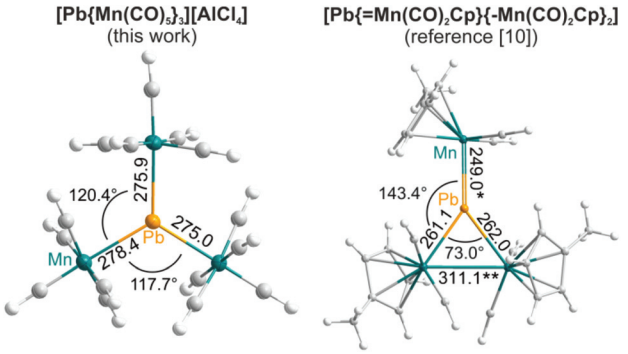

Fig. 3 Comparison of the $PbMn_3$ cluster in $[Pb\{Mn(CO)_5\}_3][AlCl_4]$ and $Pb\{Mn(CO)_2Cp\}_3$ (distances in pm; *: Pb═Mn double bond and **Mn–Mn single bond).[10]

increase of the Pb^{+I}–Mn distances in $[Pb\{Mn(CO)_5\}_3][AlCl_4]$ in comparison with the Pb^0–Mn single bonds (261.1–262.0 pm) in $Pb\{Mn(CO)_2Cp\}_3$ can be related to the steric hindrance of the CO ligands (Fig. 3).[10]

It needs to be noted that the $PbMn_3$ cluster in $[Pb\{Mn(CO)_5\}_3][AlCl_4]$ is significantly different from the only known $PbMn_3$ unit in $Pb\{Mn(CO)_2Cp\}_3$.[10] First of all, $[Pb\{Mn(CO)_5\}_3]^+$ contains three equalized Pb–Mn distances (Table 2), so that an almost equilateral triangle of three manganese atoms is spanned with lead in its center. In difference, $Pb\{Mn(CO)_2Cp\}_3$ shows largely different distances (Pb═Mn: 249, Pb–Mn: 261–262 pm) and Mn–Pb–Mn angles (73.0, 143.4, 143.6°) significantly deviating from 120° (Fig. 3).[10] Moreover, the title compound contains a $[Pb\{Mn(CO)_5\}_3]^+$ cation and a positively charged $PbMn_3$ unit with a formal Pb^{+I}, whereas the charge neutral $Pb\{Mn(CO)_2Cp\}_3$ contains lead in the formal oxidation state ±0. $[Pb\{Mn(CO)_5\}_3]^+$ with only six electrons (*i.e.* three Pb–Mn bonds) around the lead atom is electron deficient, for instance like BH_3, and can be considered less stable than the neutral $Pb\{Mn(CO)_2Cp\}_3$ molecule with a filled electron octet at lead.[10] In this regard, the merit of the ionic-liquid-based synthesis and its potential to obtain highly reactive compounds are again validated. The ionic-liquid-based approach is also more straightforward since simple $PbCl_2$ can be used as the starting material, whereas $Pb\{Mn(CO)_2Cp\}_3$ requires an elaborate heterocumulene derivative $Cp(CO)_2Mn{=}Pb{=}Mn(CO)_2Cp$ as the starting material.[10]

To verify the bonding situation of Pb and Mn, density functional theory (DFT) calculations were performed on a single $[Pb\{Mn(CO)_5\}_3]^+$ cation using the TPSS functional[13] in the dhf-TZVP-2c basis,[14] which includes a dhf-ECP-2c relativistic effective core potential (RECP) for Pb representing its {Kr} $4d^{10}4f^{14}$ core.[15] The calculations were performed at the scalar-relativistic one-component (1c) and quasi-relativistic two-component (2c) levels.[16]

At the 1c level, scalar relativistic effects are accounted for through the spin-free part of the RECP on Pb. A geometry optimization at this level yielded a highly symmetric equilibrium structure belonging to the point group D_3, in which all three Pb–Mn distances are equal (277.7 pm, Table 3). Harmonic vibrational frequencies were computed to confirm that the optimized structure is a minimum on the potential energy surface (Table 4).

At the 2c level, also non-scalar (*i.e.*, spin–orbit) effects were accounted for through the 2c part of the RECP on Pb. An equilibrium structure belonging to the point group C_2 was found at this level, with two equal Pb–Mn bonds of 277.7 pm and one slightly longer Pb–Mn bond of 278.1 pm. Thus, the distortion of the D_3 structure towards C_2 due to the spin–orbit interaction appears to be almost negligible. Harmonic vibrational frequencies were computed (from finite differences of analytical gradients) and confirmed that the optimized structure is a minimum.

In conclusion, spin–orbit effects play only a minor role in the $[Pb\{Mn(CO)_5\}_3]^+$ cation resulting in a similar electronic structure and bonding situation in the 1c and 2c descriptions. For example, the lowest unoccupied molecular orbital (LUMO) of the 1c calculation, which is an empty Pb $6p_z$ orbital, is virtually indistinguishable from the lowest unoccupied natural orbital obtained in the 2c-TPSS/dhf-TZVP-2c calculation (Fig. 4). The results obtained from a population analysis are also very similar at the 1c and 2c levels (Table 3). A Boys localization of the 1c occupied orbitals yielded three equivalent Pb–Mn σ bonds (Fig. 4). In summary, the bonding situation in the $[Pb\{Mn(CO)_5\}_3]^+$ cation can be clearly described with a formal charge of +1 on Pb, an empty $6p_z$ orbital, and three two-center-two-electron (2c2e) σ bonds. This view is in accordance with the results deduced from crystal structure analysis of

Table 3 Pb–Mn bond length and partial charges on Pb and Mn as obtained from Mulliken and natural population analyses (NPA) at 1c- and 2c-TPSS/dhf-TZVP-2c levels

			Mulliken		NPA	
		Pb–Mn (pm)	Pb	Mn	Pb	Mn
$[Pb\{Mn(CO)_5\}_3]^+$	1c	277.7	+0.85	−0.57	+0.88	−1.13
	2c	277.7/278.1	+0.83	−0.56	+0.82	−1.12

Table 4 Wavenumbers of the harmonic vibrational frequencies of the CO stretching modes of $[Pb\{Mn(CO)_5\}_3]^+$ as obtained at the 1c-TPSS/dhf-TZVP-2c level

Symmetry	a_1	e	a_1	e	e	a_1	a_2	e	e	a_2
$\tilde{\nu}$ (cm^{-1})	2127	2094	2058	2054	2049	2044	2043	2032	2021	2010
Intensity (%)	0	100	0	1.4	0.3	0	76	59	0.1	0.2

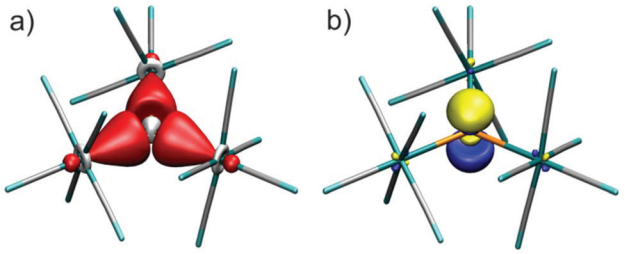

Fig. 4 Results of the DFT calculation: (a) three localized occupied molecular orbitals describing the three Pb–Mn σ bonds; (b) lowest unoccupied natural orbital (isovalue surfaces shown at $\pm 0.1\ a_0^{-3/2}$).

the aforementioned electron-deficient character of the $[Pb\{Mn(CO)_5\}_3]^+$ cation.

The Mn–C distances in the $[Pb\{Mn(CO)_5\}_3]^+$ cation range from 182.5(5) (Mn2–C10) to 188.2(5) pm (Mn2–C9) and fit well with Mn–C distances of terminal CO ligands, such as in $Mn_2(CO)_{10}$.[17] Similarly the C–O distances fit with $Mn_2(CO)_{10}$ [17] and range from 111.6(6) (C15–O15) to 113.6(6) pm (C5–O5).

In accordance with the electron-deficient character of the $[Pb\{Mn(CO)_5\}_3]^+$ cation, lead is further coordinated by two chlorine atoms as electron-pair donors of two different $[AlCl_4]^-$ anions, so that Pb – in sum – has a distorted trigonal bipyramidal coordination of three Mn and two Cl atoms (Fig. 5). Since each $[AlCl_4]^-$ anion is well coordinated to two $[Pb\{Mn(CO)_5\}_3]^+$ cations, in sum, an infinite zig-zag chain is formed (Fig. 1 and 5). Herein, the Pb–Cl distances are not equidistant, but exhibit a shorter (Pb–Cl2: 313.9(2) pm) and a longer distance (Pb–Cl1: 334.3(2) pm) (Fig. 5). The zig-zag chains exhibit Cl–Pb–Cl angles of 173.0(1)°, and they are stacked along the crystallographic *c*-axis like a hexagonal rod-type packing (Fig. 1). Compared to $PbCl_2$ (Pb–Cl: 284.7, 308.4 pm),[18] the observed Pb–Cl distances are significantly increased, which is in accordance with a formal oxidation state of Pb^{+I} and the fact that the chlorine atoms exist as $[AlCl_4]^-$, and thus, as part of a complex anion.

The $[AlCl_4]^-$ anion itself is slightly distorted from an ideal tetrahedron (Cl–Al–Cl angles: 107.0(1) to 112.5(1)°). As expected, those two Cl atoms bridging to Pb exhibit slightly longer Al–Cl distances (Al–Cl1: 215.8(2), Al–Cl2: 216.1(2) pm) compared to the two terminal Cl atoms (Al–Cl3: 210.3(2), Al–Cl4: 212.0(2) pm) (Fig. 5). This distortion points to the interaction of lead and chlorine and is often observed for asymmetric coordination (*e.g.* in $Na[AlCl_4]$).[19]

In addition to single-crystal structure analysis, the composition, structure and properties of $[Pb\{Mn(CO)_5\}_3][AlCl_4]$ were validated by energy-dispersive X-ray spectroscopy (EDXS), Fourier-transform infrared spectroscopy (FT-IR) and optical spectroscopy (UV-Vis). Accordingly, EDXS confirms a Pb : Mn : Al : Cl ratio of 1.0 : 2.6 : 1.2 : 4.0, which fits well with the composition and the calculated values (1 : 3 : 1 : 4).

FT-IR spectroscopy shows the characteristic CO vibrations with a strong absorption at 2098 cm^{-1} and three weak absorptions at 2062, 2947 and 2010 cm^{-1} (Fig. 6). In comparison with $Mn_2(CO)_{10}$,[17c] the CO vibrations of the title compound are slightly shifted to higher wavenumbers (Table 5), which, on the one hand, can be ascribed to the higher electronegativity of lead (EN(Pauling): 1.8) in comparison with manganese (EN(Pauling): 1.5),[20] and on the other hand, to the fact that manganese carries part of the positive charge in the $PbMn_3$ cluster. As a consequence, the observed CO vibrations are even more comparable to terminally bond carbonyl ligands in $Mn(CO)_5I$ or $[Pb_6I_8\{Mn(CO)_5\}_6]^{2-}$ (Table 5).[6c,21] In addition to CO vibrations, absorptions related to the ionic liquid were observed (3152–2876, 1571, 1466 cm^{-1}) and agree with reference spectra of the pure ionic liquid (Fig. 6). Finally, UV-Vis spectra of $[Pb\{Mn(CO)_5\}_3][AlCl_4]$ show a strong, continuous absorption above 450 nm as well as an absorption peak at 297 nm (Fig. 7). This finding is in accordance with the dark-red, almost black colour of single crystals (Fig. 7, inset).

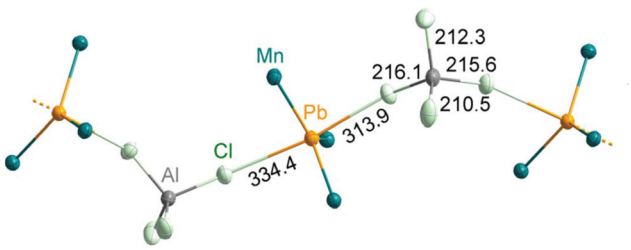

Fig. 5 Linkage of $PbMn_3$ units *via* $[AlCl_4]^-$ to infinite chains along the crystallographic *c*-axis (distances in pm; ellipsoids comprise 50% of the probability density of the atoms).

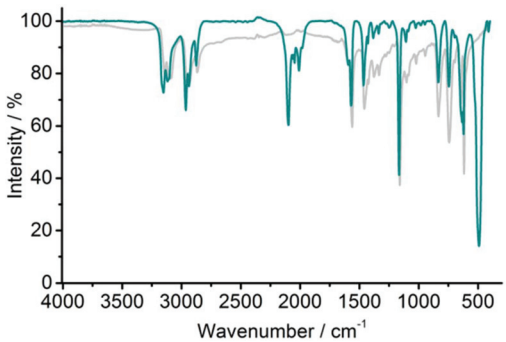

Fig. 6 FT-IR spectrum of $[Pb\{Mn(CO)_5\}_3][AlCl_4]$ (green) with the ionic liquid [BMIm][Cl] shown as a reference (grey).

Table 5 Carbonyl vibrations of $[Pb\{Mn(CO)_5\}_3][AlCl_4]$ in comparison with literature data (strong vibrations: bold)

Compound	Vibration (cm^{-1})
$[Pb\{Mn(CO)_5\}_3][AlCl_4]$ (this work)	**2098**, 2062, 2047, 2010
$Mn_2(CO)_{10}$ [17c]	**2045**, **2014**, **1983**
$Mn(CO)_5I$ [21]	2131, **2035**, **2008**, 1969
$[(Pb_6I_8)\{Mn(CO)_5\}_6]^{2-}$ [6c]	**2063**, 2008, **1964**

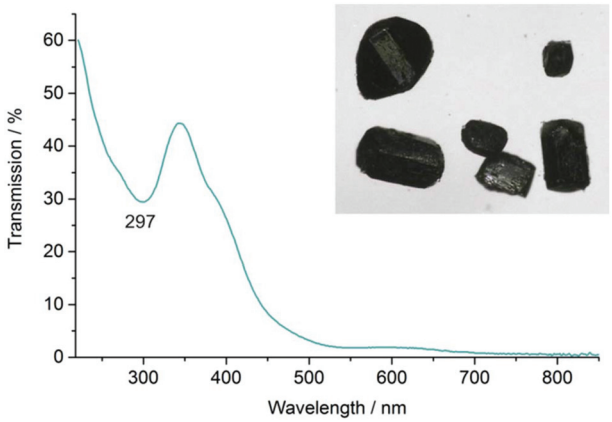

Fig. 7 UV-Vis spectrum of $[Pb\{Mn(CO)_5\}_3][AlCl_4]$ with a photo of deep red, almost black single crystals (inset).

Conclusions

The novel carbonyl cluster compound $[Pb\{Mn(CO)_5\}_3][AlCl_4]$ is presented. The title compound was prepared by the redox reaction of $PbCl_2$ and $Mn_2(CO)_{10}$ in the ionic liquid $[BMIm][AlCl_4]$ upon reduction of Pb^{+II} to Pb^{+I} and oxidation of Mn^0 to $Mn^{+I/+II}$. The $[Pb\{Mn(CO)_5\}_3]^+$ carbonyl cation contains a central $PbMn_3$ cluster with three Pb–Mn single bonds (275.0 to 278.4 pm), resulting in an almost equilateral triangle (Mn–Pb–Mn angles: 117.7(1) to 121.9(1)°) of three manganese atoms with a formal Pb^{+I} in its center. Based on the crystal structure and DFT calculations, the bonding situation in the $[Pb\{Mn(CO)_5\}_3]^+$ cation can be described with a formal charge of +1 on Pb, an empty $6p_z$ orbital, and three two-center-two-electron (2c2e) σ bonds. Similar to BH_3, thus, $[Pb\{Mn(CO)_5\}_3]^+$ represents an electron-deficient species. Such a cluster and compound were identified for the first time.

Beside the three $Mn(CO)_5$ units, the electron-deficient Pb center is further coordinated by two Cl atoms of $[AlCl_4]^-$ anions serving as electron-pair donors. Together with the triangular $PbMn_3$ cluster unit, this results in a trigonal bipyramidal coordination around Pb. Due to bidentate coordination of the $[Pb\{Mn(CO)_5\}_3]^+$ carbonyl cations as well as of the $[AlCl_4]^-$ anions, finally, infinite zig-zag chains along the crystallographic *c*-axis are formed.

The successful synthesis of the reactive carbonyl cluster can be considered as another example of the advantage of ionic-liquid-based synthesis and its promising features such as the weakly coordinating properties and the redox stability of the ionic liquids.

Experimental

Synthesis

General aspects. All reactions and sample handling were carried out under a dried argon atmosphere using standard Schlenk techniques or gloveboxes. Reactions were performed in Schlenk flasks and glass ampoules that were evacuated ($p < 10^{-3}$ mbar), heated and flashed with argon three times prior to use. The starting materials $PbCl_2$ (99.99%, ABCR), $Mn_2(CO)_{10}$ (99%, ABCR) and $AlCl_3$ (99.99%, Sigma-Aldrich) were used as received. [BMIm]Cl (99%, Iolitec) was dried under reduced pressure (10^{-3} mbar) at 130 °C for 48 h. All compounds were handled and stored in argon-filled gloveboxes (MBraun Unilab, $c(O_2, H_2O) < 0.1$ ppm).

$[Pb\{Mn(CO)_5\}_3][AlCl_4]$. 40 mg (0.144 mmol, 1 eq.) of $PbCl_2$, 96.5 mg (0.288 mmol, 2 eq.) of $Mn_2(CO)_{10}$, 500 mg (2.863 mmol) of [BMIm]Cl and 381.8 mg (2.863 mmol) of $AlCl_3$ were heated under argon in a sealed glass ampoule for 96 h at 130 °C. After cooling to room temperature with a rate of 1 K h^{-1}, the title compound was obtained as dark red crystals together with blue needles of $[Mn(CO)_6][AlCl_4]$ as a minor phase. $[Pb\{Mn(CO)_5\}_3][AlCl_4]$ is highly sensitive to air and moisture and needs to be handled under inert conditions. Since the title compound could not be obtained phase-pure, the crystals for characterization were manually separated by crystal picking.

Analytical equipment

Single-crystal X-ray structure analysis. For single crystal structure analysis, suitable crystals were selected, and covered with inert-oil (perfluoropolyalkylether, ABCR). Data collection was performed at 150 K on an Stoe Stadivari diffractometer (Stoe, Darmstadt) with Euler geometry using Ga-Kα radiation (λ = 134 pm, graded multilayer mirror as the monochromator). Data reduction and multi-scan absorption correction were conducted with the X-AREA software package (version 1.75, Stoe) and STOE LANA (version 1.63.1, Stoe).[22] Space group determination based on systematic absences of reflections, structure solution by direct methods and refinement were performed by XPREP and SHELXTL (version 6.14, SHELX-2013).[23] All atoms were refined anisotropically. Detailed information on crystal data and structure refinement is listed in Table 1. DIAMOND was used for all illustrations.[24] Further details of the crystal structure investigation may be obtained from the joint CCDC/FIZ Karlsruhe deposition service on quoting the depository number CCDC 1890307.†

Fourier-transform infrared (FT-IR) spectra were recorded on a Bruker Vertex 70 FT-IR spectrometer (Bruker). The samples were measured as pellets in KBr. Thus, 300 mg of dried KBr and 0.5–1.0 mg of the sample were carefully pestled together and pressed to a thin pellet.

Energy dispersive X-ray (EDX) analysis was performed by using an Ametec EDAX mounted on a Zeiss SEM Supra 35 VP scanning electron microscope. Samples were prepared in a glovebox by selecting single crystals that were fixed on conductive carbon pads on aluminum sample holders. Samples were handled under inert conditions during transport and sample preparation.

Optical spectroscopy (UV-Vis) of powder samples was performed on a Shimadzu UV-2700 spectrometer, equipped with an integrating sphere, in a wavelength interval of 250–800 nm against $BaSO_4$ as the reference.

Computation

Density functional theory (DFT) calculations were performed using the TPSS functional[13] in the dhf-TZVP-2c basis,[14] which includes a dhf-ECP-2c relativistic effective core potential (RECP) for Pb representing its {Kr}$4d^{10}4f^{14}$ core.[15] Version 7.4 of the TURBOMOLE program package was used.[25] Calculations were performed at the scalar-relativistic one-component (1c) and quasi-relativistic two-component (2c) levels.[16]

Conflicts of interest

There are no conflicts to declare.

Acknowledgements

The authors acknowledge the Deutsche Forschungsgemeinschaft (DFG) for funding in the Priority Program SPP1708 "Synthesis near room temperature".

Notes and references

1 (*a*) P. Wasserscheid and T. Welton, *Ionic Liquids in Synthesis*, Wiley-VCH, Weinheim, 2008; (*b*) D. Freudenmann, S. Wolf, M. Wolff and C. Feldmann, *Angew. Chem., Int. Ed.*, 2011, **50**, 11050 (Review). (*c*) M. F. Groh, A. Wolff, M. A. Grasser and M. Ruck, *Int. J. Mol. Sci.*, 2016, **17**, 1452.

2 A. M. Guloy, R. Ramlau, Z. Tang, W. Schnelle, M. Baitinger and Y. Grin, *Nature*, 2006, **443**, 320.

3 (*a*) S. Santner and S. Dehnen, *Inorg. Chem.*, 2015, **54**, 1188; (*b*) R. J. Wilson, F. Hastreiter, K. Reiter, P. Büschelberger, R. Wolf, R. Gschwind, F. Weigend and S. Dehnen, *Angew. Chem., Int. Ed.*, 2018, **57**, 15359.

4 M. Knies, M. Kaiser, A. Isaeva, U. Müller, T. Doert and M. Ruck, *Chem. – Eur. J.*, 2018, **24**, 127 (Review).

5 I. M. Riddlestone, A. Kraft, J. Schaefer and I. Krossing, *Angew. Chem., Int. Ed.*, 2018, **57**, 13982.

6 (*a*) S. Wolf, F. Winter, R. Pöttgen, N. Middendorf, W. Klopper and C. Feldmann, *Chem. – Eur. J.*, 2012, **18**, 13600; (*b*) S. Wolf, W. Klopper and C. Feldmann, *Chem. Commun.*, 2018, **54**, 1217; (*c*) S. Wolf, K. Reiter, F. Weigend, W. Klopper and C. Feldmann, *Inorg. Chem.*, 2015, **54**, 3989.

7 (*a*) S. Wolf, F. Winter, R. Pöttgen, N. Middendorf, W. Klopper and C. Feldmann, *Dalton Trans.*, 2012, **41**, 10605; (*b*) S. Wolf and C. Feldmann, *Z. Anorg. Allg. Chem.*, 2017, **643**, 25.

8 P. Braunstein, L. A. Oro and P. R. Raithby, *Metal Clusters in Chemistry*, Wiley-VCH, Weinheim, 2008.

9 (*a*) F. Ettel, G. Hutter and L. Zsolnai, *Angew. Chem., Int. Ed. Engl.*, 1989, **28**, 1496; (*b*) F. Ettel, M. Schollenberger, B. Schiemenz, W. Imhof, G. Huttner and L. J. Zsolnai, *Organomet. Chem.*, 1994, **476**, 207; (*c*) F. Ettel, M. Schollenberger, B. Schiemenz, G. Huttner and L. J. Zsolnai, *Organomet. Chem.*, 1994, **476**, 153; (*d*) V. S. Leong and N. J. Cooper, *Organometallics*, 1988, **7**, 2080.

10 H.-J. Kneuper, E. Herdtweck and W. A. Herrmann, *J. Am. Chem. Soc.*, 1987, **109**, 2508–2509.

11 (*a*) H. J. Haupt, W. Schubert and F. Huber, *J. Organomet. Chem.*, 1973, **54**, 231; (*b*) M. R. Brooth, D. J. Cardin, N. A. D. Carey, H. C. Clark and B. R. Sreenathan, *J. Organomet. Chem.*, 1970, **21**, 171.

12 (*a*) E. O. Fischer and K. Öfele, *Angew. Chem.*, 1961, **73**, 581; (*b*) E. O. Fischer, K. Fichtel and K. Öfele, *Chem. Ber.*, 1962, **95**, 249.

13 J. Tao, J. P. Perdew, V. N. Staroverov and G. E. Scuseria, *Phys. Rev. Lett.*, 2003, **91**, 146401.

14 M. K. Armbruster, W. Klopper and F. Weigend, *Phys. Chem. Chem. Phys.*, 2006, **8**, 4862.

15 B. Metz, H. Stoll and M. Dolg, *J. Chem. Phys.*, 2000, **113**, 2563.

16 M. K. Armbruster, F. Weigend, C. van Wüllen and W. Klopper, *Phys. Chem. Chem. Phys.*, 2008, **10**, 1748.

17 (*a*) L. F. Dahl and R. E. Rundle, *Acta Crystallogr.*, 1963, **16**, 419; (*b*) M. R. Churchill, K. N. Amoh and H. J. Wasserman, *Inorg. Chem.*, 1981, **20**, 1609; (*c*) H. Haas and R. K. J. Sheline, *Chem. Phys.*, 1967, **47**, 2996.

18 M. Lumbreras, J. Protas, S. Jebbari, G. J. Dirksen and J. Schoonman, *Solid State Ionics*, 1986, **20**, 295.

19 W. Scheinert and A. Weiss, *Z. Naturforsch., A: Phys., Phys. Chem., Kosmophys.*, 1976, **31**, 1354.

20 J. E. Huheey, E. A. Keiter, R. L. Keiter and O. K. Medhi, *Inorganic Chemistry: Principles of Structure and Reactivity*, Pearson, Cambridge, 2008.

21 H. Li and I. S. Butler, *Appl. Spectrosc.*, 1992, **46**, 1785.

22 J. Koziskova, F. Hahn, J. Richter and J. Kozisek, *Acta Chim. Slovaca*, 2016, **9**, 136.

23 (*a*) G. M. Sheldrick, *Acta Crystallogr., Sect. A: Found. Crystallogr.*, 2008, **64**, 112; (*b*) G. M. Sheldrick, *Acta Crystallogr., Sect. C: Struct. Chem.*, 2015, **71**, 3.

24 *DIAMOND Version 4.2.2: Crystal and Molecular Structure Visualization*, Crystal Impact GbR, Bonn, 2016.

25 TURBOMOLE V7.4 2019, a development of University of Karlsruhe and Forschungszentrum Karlsruhe GmbH, 1989–2007, TURBOMOLE GmbH, since 2007; available from http://www.turbomole.com.